Journal of Nanobiotechnology

RESEARCH

Open Access

Tumor targeting peptide TMTP1 modified Antigen capture Nano-vaccine combined with chemotherapy and PD-L1 blockade effectively inhibits growth of ovarian cancer

Ying Zhou[1,2†], Rui Wei[1,2†], Ling Wang[3], Jie Li[1,2], Wei Wang[1,2], Guiying Jiang[4], Songwei Tan[5], Fei Li[1,2], Xueqian Wang[1,2], Xiangyi Ma[1,2*] and Ling Xi[1,2*]

Abstract

The mortality of ovarian cancer (OC) has long been the highest among gynecological malignancies. Although OC is considered to be an immunogenic tumor, the effect of immunotherapy is not satisfactory. The immunosuppressive microenvironment is one reason for this, and the absence of recognized effective antigens for vaccines is another. Chemotherapy, as one of the most commonly used treatment for OC, can produce chemotherapy-associated antigens (CAAs) during treatment and show the effect of in situ vaccine. Herein, we designed an antigen capture nano-vaccine NP-TP1@M-M with tumor targeting peptide TMTP1 and dendritic cell (DC) receptor mannose assembled on the surface and adjuvant monophosphoryl lipid A (MPLA) encapsulated in the core of poly (D, L-lactide-co-glycolide) (PLGA) nanoparticles. PLGA itself possessed the ability of antigen capture. TMTP1 was a tumor-homing peptide screened by our research team, which held extensive and excellent tumor targeting ability. After these modifications, NP-TP1@M-M could capture and enrich more tumor-specific antigens after chemotherapy, stimulate DC maturation, activate the adaptive immunity and combined with immune checkpoint blockade to maximize the release of the body's immune potential, providing an eutherapeutic strategy for the treatment of OC.

Keywords Cancer vaccine, Nano-vaccine, TMTP1, Antigen capture, Combination therapy, Ovarian cancer

†Ying Zhou and Rui Wei contributed equally to this work.

*Correspondence:
Xiangyi Ma
xyma@tjh.tjmu.edu.cn
Ling Xi
lxi@tjh.tjmu.edu.cn
[1]Department of Gynecological Oncology, Tongji Hospital, Tongji Medical College, Huazhong University of Science and Technology, Wuhan, China
[2]National Clinical Research Center for Obstetrics and Gynecology, Cancer Biology Research Center (Key Laboratory of the Ministry of Education), Tongji Hospital, Tongji Medical College, Huazhong University of Science and Technology, Wuhan, China
[3]Department of Obstetrics and Gynecology, the First Affiliated Hospital of Anhui Medical University, Hefei, China
[4]Department of Obstetrics and Gynecology, West China Second Hospital, Sichuan University, Chengdu, China
[5]Tongji School of Pharmacy, Tongji Medical College, Huazhong University of Science and Technology, Wuhan, China

Ovarian cancer (OC) is the most malignant gynecological tumor at present. The 5-year survival rate maintains around 30-40% for a long time due to occult onset, chemotherapy resistance, and unsatisfied immunotherapy [1]. OC is considered as an immunogenic tumor that can be recognized by the host immune system. Tumor-reactive T cells and antibodies generated by spontaneous antitumor immune response can be detected in the peripheral blood, tumor tissues and ascites of patients with OC [2]. These results indicate that immunotherapy could be a highly promising approach for OC therapy. However, several clinical trials indicated that the most commonly used immune checkpoint blockade had an average response rate of only 10-15% in OC [3–6]. Adoptive T-cell therapy demands complex and costly technical processes. The first study of adoptive transfer of folate receptor-α chimeric antigen receptors (CARs) in OC showed no clinical response [7]. Therapeutic cancer vaccines are the most studied immunotherapeutic strategy in OC [8]. Unfortunately, there is no recognized and effective antigen for the design of OC vaccines in clinical trials due to the prominent molecular heterogeneity in ovarian cancer [9]. Paijens et al. also found that there was no clinically effective antigen-specific active immunotherapy for OC by summarizing 67 related clinical trials in OC [10]. Much effort is needed to improve the performance of cancer vaccines in OC.

In general, tumor vaccines consist of three main components: tumor antigen, immune adjuvant and delivery system. Optimizing the selection of individual tumor antigens, collocating with safe and effective vaccine adjuvants, and assembling an efficient delivery system, all these could improve the therapeutic effect of tumor vaccine. With the spring up of nanotechnology, nanocarriers have a broad prospect in the design of tumor vaccines. Nano-vaccines containing tumor antigens and adjuvants were widely studied due to their superior stability, increased uptake rate by antigen-presenting cells, and enhanced antigen presentation efficiency [11]. Particularly, vaccine delivery system based on poly (D, L-lactide-co-glycolide) (PLGA) presented a promising prospect of application due to its excellent safety profile and biodegradability [12]. For instance, Yang et al. used PLGA loaded with adjuvant toll-like receptor 7 agonist, imiquimod (R837) and coated with cancer cell membranes to develop a nano-vaccine which showed great efficacy to delay tumor progression [13]. Koerner et al. developed a PLGA-particle vaccine carrying toll-like receptor 3 (TLR3)/retinoic acid-inducible gene I (RIG-I) ligand Riboxxim which afforded primary tumor growth retardation, prevention of metastases, and prolonged survival in preclinical tumor models [14]. More surprisingly, recent studies shown that PLGA nanoparticle (NP) itself had antigen-capturing (AC) properties, which could capture tumor antigens released after radiotherapy and served as in situ vaccine, demonstrated improved abscopal effect and cancer immunotherapy [15]. In fact, only a small fraction of the membrane proteins in tumor cell lysis products are immunogenic, leading to the fact that vaccines designed using whole tumor cells fail to provide significant long-term therapeutic benefits [16]. Therefore, if we make some modifications on the surface of PLGA NPs with structures that could specifically capture tumor associated antigens, then its immune activation effect will be better.

TMTP1 is a tumor-homing peptide screened by FliTrx bacterial peptide display system [17]. Previous studies have shown that TMTP1 can target to multiple primary tumors and metastases, including prostate cancer, lung cancer, breast cancer, gastric cancer, hepatocellular cancer, ovarian cancer and cervical cancer [17–23]. PLGA NPs modified with TMTP1 on the surface and coated with near infrared fluorescence imaging agent indocyanine green (ICG) could specifically image cervical cancer foci and lymph node metastases [24]. TMTP1-Modified, tumor microenvironment responsive NPs co-deliver cisplatin and paclitaxel prodrugs significantly improved the therapeutic efficacy of the traditional cisplatin–paclitaxel combination chemotherapy [25]. Research found that some polypeptide could bind with specific small molecular protein produced by tumors to affect tumor microenvironment. Peptides can also be used as scaffold for assembly and epitope presentation in vaccines based on tumor associated antigens, such as self-adjuvanting vaccines [26]. In fact, the use of peptide-modified vectors to capture specific proteins or cells has been widely studied [27–29]. Due to the extensive and excellent tumor targeting ability of TMTP1, we speculated that TMTP1 modified PLGA NP could capture and enrich tumor specific antigens and increase the immunogenicity of tumor vaccine.

Chemotherapy is one of the most commonly used treatment options for OC patients, which is usually combined chemotherapy based on platinum drugs. Current studies have shown that chemotherapy could induce tumor cell lysis and death, producing a large number of damage-associated molecular patterns (DAMPs) [30]. These tumor lysis fragments and DAMPs are immunogenic and thus become in situ vaccines. Marino et al. identified chemotherapy-associated antigens (CAAs) in OC and these CAAs could elicit the response of effector T cells [31]. However, these free tumor antigens are usually limited. On the one hand, the CAAs have relatively poor immunogenicity and are not sufficient to induce T cell response. On the other hand, the presence of a large number of regulatory T cells (Tregs) suppresses the immune response [32]. Therefore, we designed TMTP1 modified antigen capture nano-vaccine to enrich the

CAAs and increase the immunogenicity, thus promoting the downstream immune response. In addition, adjuvants have been clearly shown to increase immunogenicity, among which monophosphoryl lipid A (MPLA) is one of the most promising adjuvants and has been widely used in vaccine design [33]. And MPLA could be easily encapsulated in PLGA NPs due to its lipid solubility. Mannose is a receptor of dendritic cell (DC), and mannose modified vaccine can be more easily recognized and ingested by DC [13, 34]. In this study, the target nano-vaccine was encapsulated MPLA in the core and modified mannose on the surface to enhance the uptake of DC. For immunosuppression, we combined immune checkpoint blockade (ICB) therapy.

Herein, we hoped to design a nano-vaccine (NP-TP1@M-M) with tumor targeting peptide TMTP1 and DC receptor mannose assembled on the surface of PLGA NPs and adjuvant MPLA encapsulated in the core for the treatment of OC after chemotherapy. Schematic illustration of nano-vaccine synthesis and the combination therapy mechanism was shown in Fig. 1. This novel nano-vaccine could capture tumor antigens after chemotherapy and stimulate DC maturation, then combined with ICB (aPD-L1) to maximize the release of the body's immune potential, providing a new strategy for the treatment of OC.

Results and discussion

NP-TP1@M-M Was constructed and the TMTP1 / mannose modification ratio was determined to be 1:2

In our previous study, we synthesized the precursor material PLGA-PEG-TMTP1 by linking PLGA-PEG-Mal

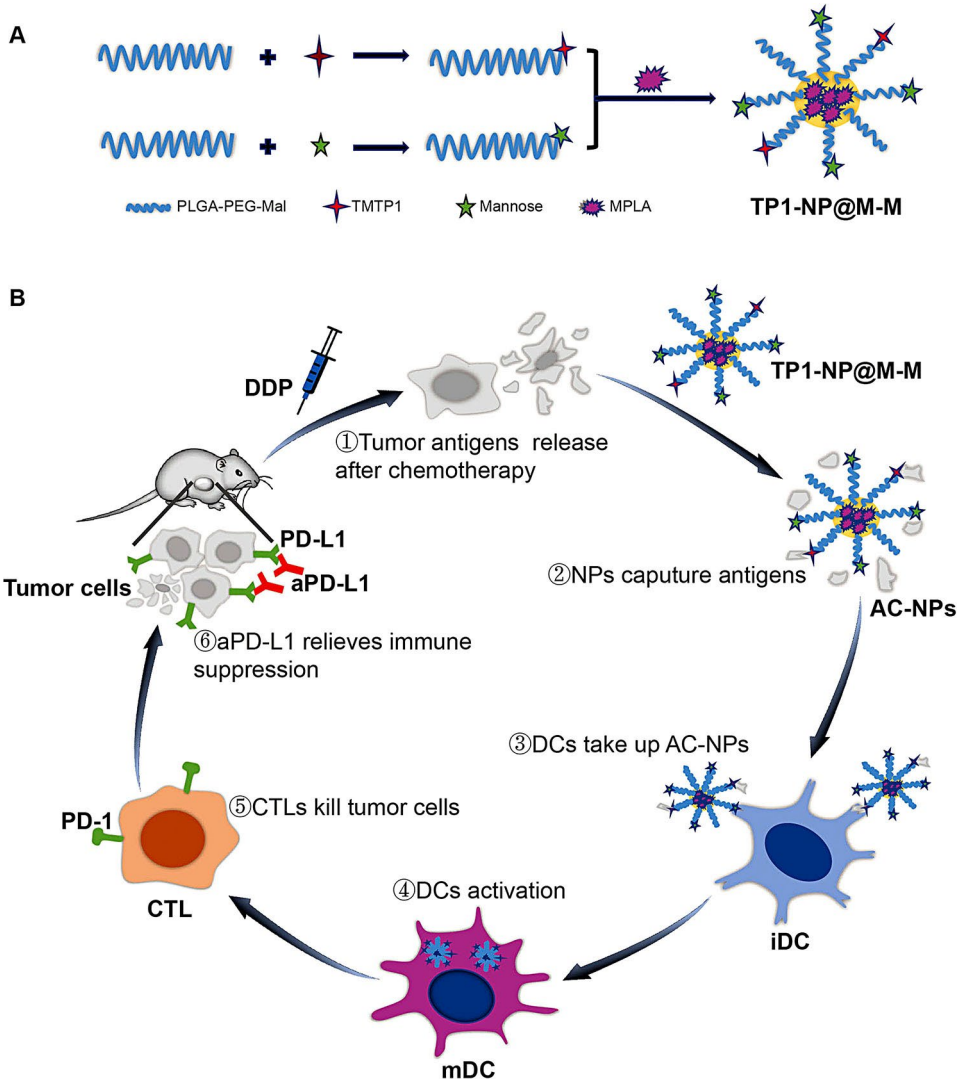

Fig. 1 Schematic illustration of nano-vaccine synthesis and the combination therapy mechanism. (**A**) Schematic diagram of preparation of nano-vaccine NP-TP1@M-M. (**B**) Schematic illustration of antitumor immunity principle induced by nano-vaccine NP-TP1@M-M in combination with chemotherapy and immune checkpoint blockade

A

Effective Diameter (nm)

NPs (TMTP1: Mannose)	TP1	AC-TP1
1:2	120	142.1
1:1	120.3	138.2
2:1	119.2	132.8
NPs (mPEG: Mannose)	CON	AC-CON
1:2	134.4	138.5
1:1	131.4	133.3
2:1	127.7	137.4

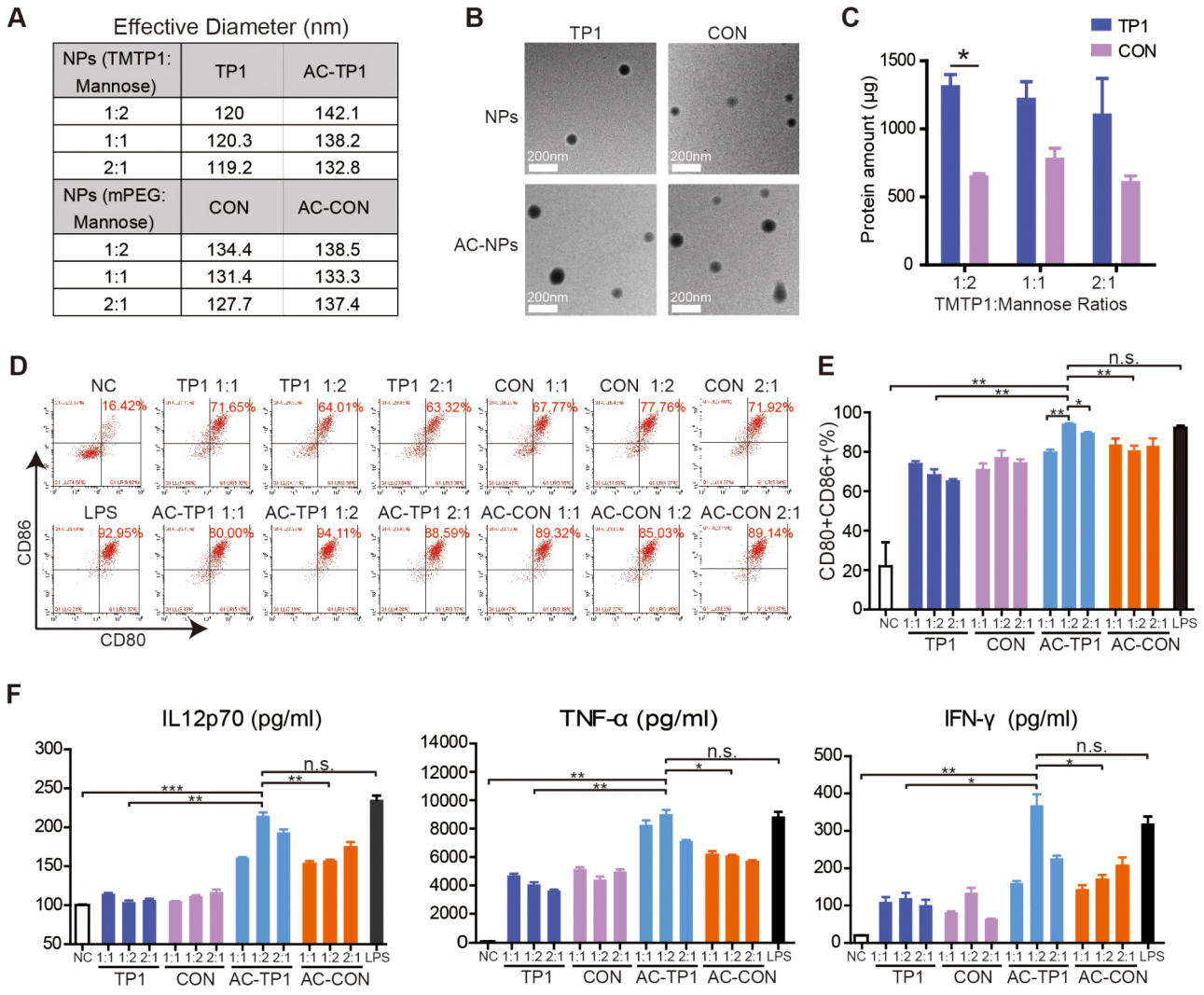

Fig. 2 Characterization of nano-vaccines. (**A**) The average hydrodynamic diameters of TP1-NPs, AC-TP1-NPs, CON-NPs and AC-CON-NPs at different ratios of TMTP1 to mannose. (**B**) The representative TEM images of these NPs when the ratio of TMTP1 to mannose was 1:2. (**C**) The total protein amount captured by TP1-NPs and CON-NPs of different TMTP1 to mannose ratios. (**D**) Representative flow cytometry data to show DC maturation induced by different formulations of NPs or AC-NPs. (**E**) The corresponding statistics of Fig. 2D. (**F**) Secretion levels of proinflammatory cytokine IL-12p70、TNF-α、IFN-γ after stimulation by these NPs or AC-NPs. (***$P < 0.001$, **$P < 0.01$ or *$P < 0.05$.)

with TMTP1 [24]. Similarly, maleimide group of PLGA-PEG-Mal and mannosamine were synthesized into mannose-modified precursor material PLGA-PEG-Man by addition reaction, and further confirmed by ^{1}H NMR spectrum (Figure S1). Then adjust the ratio of the two and add MPLA to prepare NP-TP1@M-M (Fig. 1A). By adjusting the ratio of TMTP1 to mannose to be 1:2, 1:1 and 2:1, we successfully synthesized three kinds of nano-vaccines, recorded as TP1-NPs. The control materials mPEG2000-PLGA and PLGA-PEG-Man were used to synthesize three kinds of control nano-vaccines, denoted as CON-NPs. To prepare AC-NPs, TP1-NPs or CON-NPs was incubated with the tumor antigens from ID8 cells after chemotherapy in vitro.

The average hydrodynamic diameters of TP1-NPs, AC-TP1-NPs, CON-NPs and AC-CON-NPs detected by dynamic light scattering (DLS) were shown in Fig. 2A. The diameters of TP1-NPs of all proportions were about 120 nm, and the diameters of AC-TP1-NPs increased slightly after antigen capture. CON-NPs showed similar properties, but with less diameter increase after antigen capture. The representative transmission electron microscopy (TEM) images of the 1:2 NPs were displayed on Fig. 2B, which further confirmed the size distribution and sphere-like morphologies of these NPs. TEM showed that the particle size was slightly smaller than the hydration particle size, which was of the optimal size (around 100 nm) for LN targeted delivery [35, 36]. In addition, we calculated the total amount of proteins captured by

TP1-NPs and CON-NPs by detecting the difference of protein amount before and after incubation with antigen solution, as shown in Fig. 2C. Overall, TP1-NPs captured more proteins than CON-NPs, and the difference of total protein amount between nanoparticles with a 1:2 ratio was statistically significant, suggesting that TP1-NP with this ratio might capture the most amount of tumor antigens.

The immature DCs could be stimulated into the matured status by antigens, leading to antigen presentation and further activate T cells and induce the subsequent immune responses [37]. Then we stimulated immature bone marrow-derived dendritic cells (BMDCs) with these NPs and AC-NPs, lipopolysaccharide (LPS) as positive control, and no stimulus as the negative control (NC). The results showed that the proportion of mature DCs (CD11c+CD80+CD86+) stimulated by nanoparticles was mostly between the NC group and LPS group (Fig. 2D). On the whole, the proportion of mature DC stimulated by AC-NPs was higher than that stimulated by NPs, which might be related to the tumor antigens contained in AC-NPs (Fig. 2E). In addition, the CON-NPs showed comparable stimulative effect to that of TP1-NPs but stronger than that of NC group, which might be due to the stimulating effect of adjuvant MPLA on DC and the immunogenicity of nanoparticles themselves [11]. We also detected the levels of IL-12p70, TNF-α and IFN-γ in the BMDC supernatant after stimulation, as shown in Fig. 2F. The results showed that AC-TP1-NPs, especially when the ratio of TMTP1 to mannose was 1:2, could promote more DC maturation and stimulate BMDC to release more proinflammatory cytokines than TP1-NPs and AC-CON-NPs, and the stimulation effect was comparable to that of the positive control LPS (Fig. 2E and F). As a commonly used vaccine adjuvant, MPLA itself can stimulate DC. Further, we conducted experiments to compare the stimulative effects of MPLA alone, MPLA-free TP1-NP@M, MPLA-loading TP1-NP@M-M and tumor antigen captured AC-TP1-NP@M-M on BMDCs. The TMTP1/Mannose modification ratio of nanoparticles in this experiment was 1:2. The results displayed on Figure S2. The proportion of mature DC stimulated by TP1-NP@M-M was higher than that stimulated by MPLA alone or MPLA-free TP1-NP@M. MPLA or TP1-NP@M alone could also significantly promote DC maturation, compared with NC. These results collectively demonstrated that AC-TP1-NPs which captured the tumor antigens from ID8 cells after chemotherapy could promote DC maturation and increase proinflammatory cytokine secretion. Based on the above results, we chose NPs with a 1:2 ratio of TMTP1: Mannose for subsequent experiments. More TMTP1-modified nanoparticles may instead lead to less antigen capture due to space crowding or lower efficiency. Actually, similar observation has been reported in previously studies. For example, Christopher W. Cairo concluded that ligands with low binding epitope density, however, were the most efficient on a binding epitope basis in a study of multivalent interactions by binding epitope density [38]. On a molecular basis, the most efficient compounds are those bearing the lowest ligand densities whereas higher ligand densities convey the largest ligand-receptor clusters [39]. Similarly, in a design of cyclic RGDyK conjugated polymeric micelles to promote drug uptake of integrin overexpressing tumor cells, concluded that there was not positive correlation between the ligand conjugation density on the surfaces of micelles and the cellular uptake [40].

Protein sequencing further confirmed that NP-TP1@M-M could capture more tumor antigens after chemotherapy

We prepared nano-vaccine AC-NPs which captured chemotherapy-associated tumor antigens and used label free relative quantitative method for protein spectrum detection. As shown in Fig. 3A and B and Table S1, AC-TP1-NP group contained 2953 types of proteins and AC-CON-NP contained 2490 types of proteins, of which 2401 types were both contained, 552 types were unique to AC-TP-NP, and 89 types were unique to AC-CON-NP. Proteins with ≥2 unique peptide were identified with greater confidence, with a total of 2299 proteins (bold numbers in Fig. 3A), including 2108 proteins that both contained, 196 specific to AC-TP1-NP group, and 9 specific to AC-CON-NP group. These results indicated that the total and specific categories of proteins captured by AC-TP1-NP were higher than those of AC-CON-NP. Further quantitative analysis was conducted to find the different proteins in the two group, and it was found that the total number of up-regulated proteins of AC-TP1 vs. AC-CON was 432, while 69 were down-regulated (Table S2). Then we analyzed the abundance of tumor antigens we detected by referring to tumor neoantigens, DAMPs and CAAs of OC listed in previous studies [30, 31, 41]. As shown in Fig. 3C, there were 8 matched neoantigens among the detected proteins, and 3 of them had higher abundance in AC-TP1-NP (Ratio≥4), of which Dag1 and Tubb3 were specific to AC-TP1-NP. For DAMPs, Hspa12a and Hspa14 had significantly higher abundance in AC-TP1-NP and Hspa14 was unique to AC-TP1-NP. Among the CAAs, Zfp36l2 was unique to AC-TP1-NP. It followed that the abundance of tumor antigen captured by TP1-NP was significantly higher than that of CON-NP. Although several studies had shown the antigen-capturing ability of nanoplatforms, [15, 42, 43] NP-TP1@M-M in this study showed outstanding advantages in both the type and abundance of the captured antigen proteins.

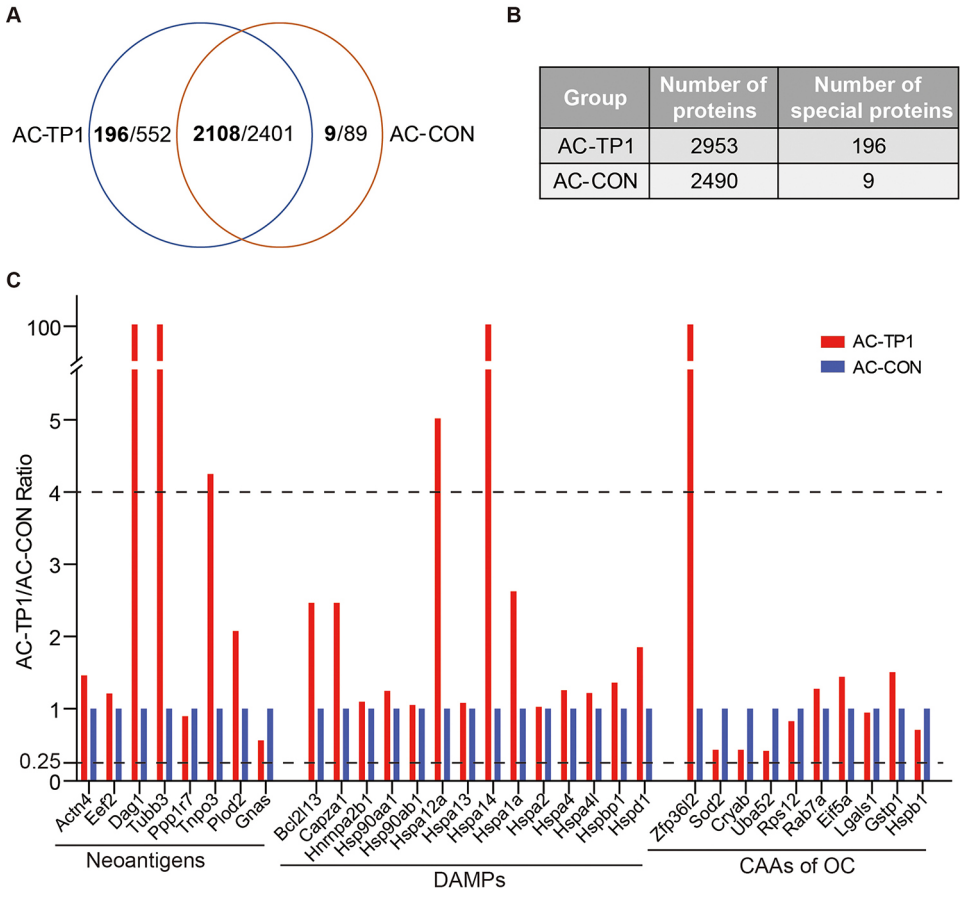

Group	Number of proteins	Number of special proteins
AC-TP1	2953	196
AC-CON	2490	9

Fig. 3 Protein captures in vitro of nano-vaccines by mass spectrometry. (**A**) Qualitative results of proteins captured by AC-TP1-NP and AC-CON-NP, with bold numbers representing the number of proteins with a unique peptide number ≥ 2. (**B**) The total number of proteins and specific proteins captured by AC-TP1-NP and AC-CON-NP. (**C**) Quantitative analysis of neoantigens, DAMPs and CAAs of OC in captured proteins. AC-TP1/AC-CON Ratio is the ratio of peak intensity of unique peptide segment of each protein

NP-TP1@M-M after antigen capture led to more uptake by DC in vitro

NPs and AC-NPs containing green fluorescent dye coumarin-6 were successfully synthesized and incubated with DC2.4 cells to detect the uptake of nanoparticles by DC. As shown in Fig. 4A, the green fluorescence intensity of AC-NPs was significantly stronger than that of NPs, indicating that the uptake of antigen-captured nanoparticles by DCs was significantly increased than that of antigen-free nanoparticles. In addition, the green fluorescence intensity of AC-TP1-NP was stronger than AC-CON-NP, indicating that AC-TP1-NP was more easily taken up by DCs than the control NP. Flow cytometry was also performed on the incubated cells (Fig. 4B), and the peak value of fluorescence intensity of AC-TP1-NP group shifted to the right significantly, further illustrating this result. Additionally, the concentration gradient nanoparticles were incubated with DC2.4 cells for 48 h, and their toxicity to DC2.4 cells was detected by CCK-8 test. The results were shown in Fig. 4C, the activity of DC2.4 cells remained about 100% under various concentrations, indicating that neither NPs nor AC-NPs had significant toxicity to DCs. These results suggested that NP-TP1@M-M was safe and led to more uptake by DC after antigen capture, which was crucial for tumor antigen presentation [44].

NP-TP1@M-M could significantly drain to lymph nodes in vivo

NPs labeled with fluorescent dye DiR and free DiR were injected locally into the footpads of C57BL/6 mice to detect lymph node drainage in vivo. DiR is a kind of near infrared (NIR) fluorescent dye with fat solubility, which can be easily encapsulated in PLGA nanoparticles and suitable for in vivo imaging [45]. Fluorescence images collected by living imaging system after drug administration were displayed in Fig. 5A. The mice were sacrificed 4 h after administration, and the fluorescence images of isolated lymph nodes and major organs were presented in Fig. 5B. The region of interest (ROI) tool in the IVIS imaging software was used to measure the fluorescence radiation at lymph nodes, and the fluorescence

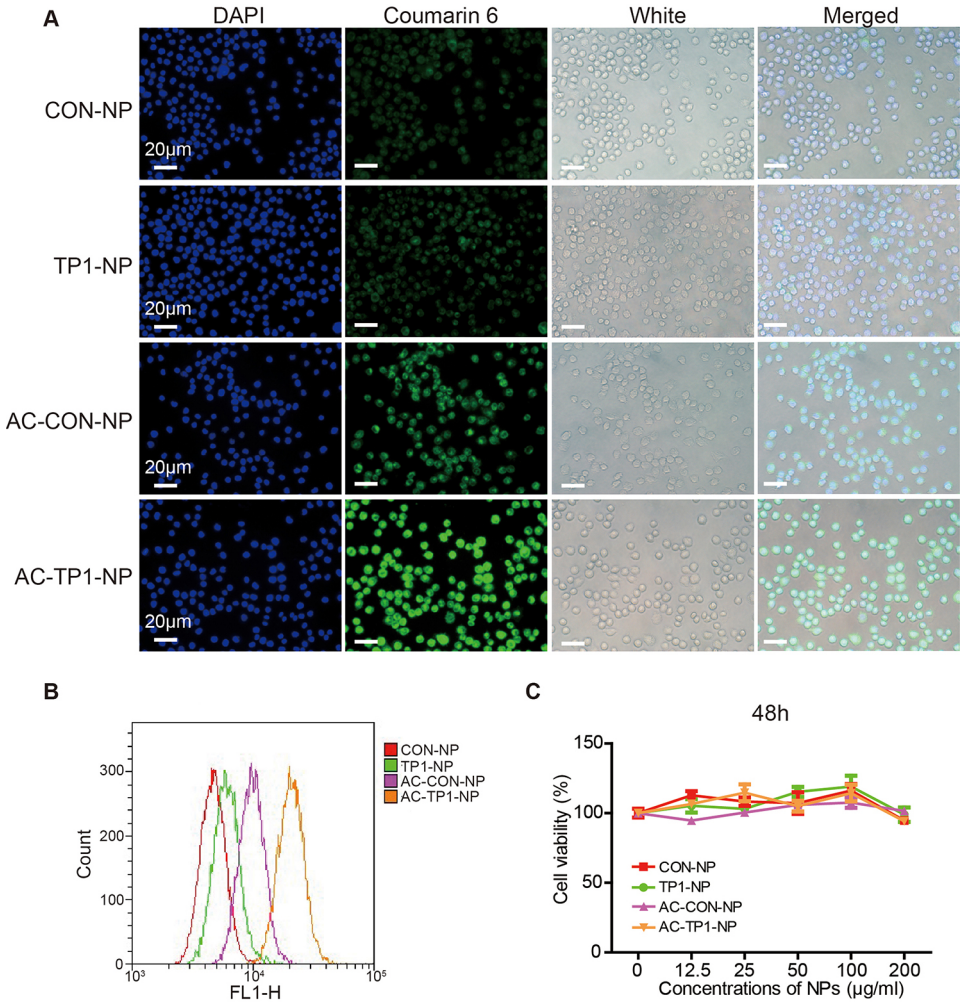

Fig. 4 DC cellular uptake and toxicity of nano-vaccines. (**A**) Fluorescence and white images of DC2.4 cells treated with coumarin-6 labeled NPs and AC-NPs. (**B**) Green fluorescence intensity of DC2.4 cells in (**A**) by flow cytometry. (**C**) Cell activity of DC2.4 cells after incubation with concentration gradient nanoparticles (12.5, 25, 50, 100, 200 μg/ml)

radiance curve over time was illustrated in Fig. 5C. All the nanoparticles could be obviously drained to lymph nodes. Obviously, the nanoparticles drained to lymph nodes in each group was significantly higher than DiR. These results indicated that these nanoparticles were easy to accumulate in lymph nodes, which was consistent with the characteristics of nanoparticles themselves. It could be found that the fluorescence intensity of AC-NPs group was higher than that of the CON-NP group, and the fluorescence intensity in the lymph nodes of the TP1-NP group was also significantly stronger than that of the CON-NP group. This may be related to the size, morphology and surface modification of TP1-NP, and the change of physical properties of nanoparticles could also affect the efficiency of lymph node drainage [36].

Antitumor effect of NP-TP1@M-M combined with chemotherapy and immune checkpoint blockade

ID8 ovarian cancer cells were implanted into the abdominal cavity of C57BL/6 mice to build the abdominal metastasis model of OC, and then the mice were treated with the combination of chemotherapy (Cisplatin, DDP), nano-vaccine, and immune checkpoint blockade (aPD-L1) for three cycles of administration, as shown in Fig. 6A. In this study, we supposed that NP-TP1@M-M could capture and enrich tumor-specific antigens after chemotherapy, and then stimulate DC maturation, enhance anti-tumor immune response. Chemotherapy is the most important adjuvant treatment for ovarian cancer patients in clinical practice and chemotherapy is recommended for all high-grade serous ovarian cancer [46]. Therefore, we set the combination of TP1-NP and DDP as the experimental group in the design of animal experiments, without a TP1-NP only group. PD-L1 was found to be highly expressed in OC patients [47]. Besides

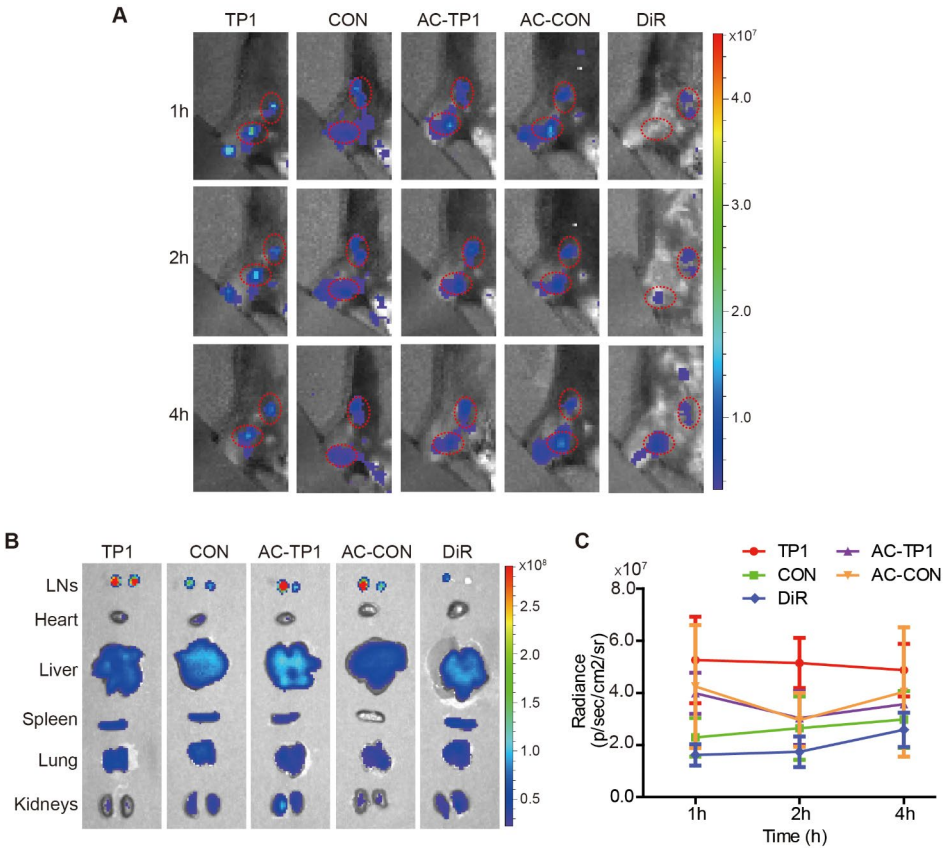

Fig. 5 Lymph node drainage of nano-vaccines. (**A**) Fluorescence images of mice 1 h, 2 h and 4 h after local injection of DiR labeled NPs and AC-NPs. The red circles marked the draining lymph nodes, including popliteal and inguinal lymph nodes. (**B**) Fluorescence images of isolated lymph nodes and major organs 4 h after the administration of nano-vaccines. (**C**) Quantitative fluorescence signals at the draining lymph nodes based on in vivo imaging data shown in (**A**)

tumor cells, PD-L1 was also expressed in tumor-associated macrophages (TAMs) and immunosuppressive DC subsets [48]. Therefore, we speculated that PD-L1 blockers were more effective than other ICBs in improving the immunosuppressive microenvironment of OC. We respectively explored the therapeutic effects of the combination of nano-vaccine and DDP, as well as the addition of aPD-L1, grouping shown in Fig. 6B. ID8 cells were tagged with luciferase to monitor tumor growth under the IVIS imaging system. Photos were taken every two weeks after tumor implantation, and the results were shown in Fig. 6B. The ROI tool of imaging software was used to measure the abdominal fluorescence intensity of each mouse at each time point, as presented in Fig. 6C. Obviously, the growth rate of abdominal tumor in TP1+DDP+aPD-L1 group was obviously slower than that in other groups. Tumor growth was also slower in TP1+DDP group than in CON+DDP group and PBS+DDP group. We observed 180 days after tumor implantation, and the survival curve was displayed in Fig. 6D. TP1+DDP+aPD-L1 group exhibited the best survival rate. The survival of TP1+DDP group was also better than that of CON+DDP group and PBS+DDP group. These results indicated that TP1-NP combined chemotherapy had better therapeutic effect than CON-NP or chemotherapy alone. When aPD-L1 was added, the therapeutic effect was further improved, with 37.5% of the mice surviving more than 180 days. To detect immune activation, lymph node and spleen tissues were collected 7 days after the end of administration for lymphocyte isolation and flow cytometry. Both the mice of TP1+DDP group and TP1+DDP+aPD-L1 group showed increased percentage of active DCs in lymph node (Figure S3). TP1+DDP+aPD-L1 group also had a higher proportion of CD4+T cells (CD3+CD4+) cells and CD8+T cells (CD3+CD8+) cells and a lower proportion of Treg (CD3+CD4+Foxp3+) cells in lymph node (Figure S4). In addition to the proportion of CD4+and CD8+T cells, we also measured the proportion of IFN-γ producing CD8+cytotoxic T lymphocytes in spleen. Consistently, either the TP1+DDP group or the TP1+DDP+aPD-L1 group had more CD4+T cells, CD8+T cells, and CD8+IFN-γ+T cells than the corresponding control group (Figure S5). These results suggested that nano-vaccine NP-TP1@M-M could promote DC activation after chemotherapy and enhance

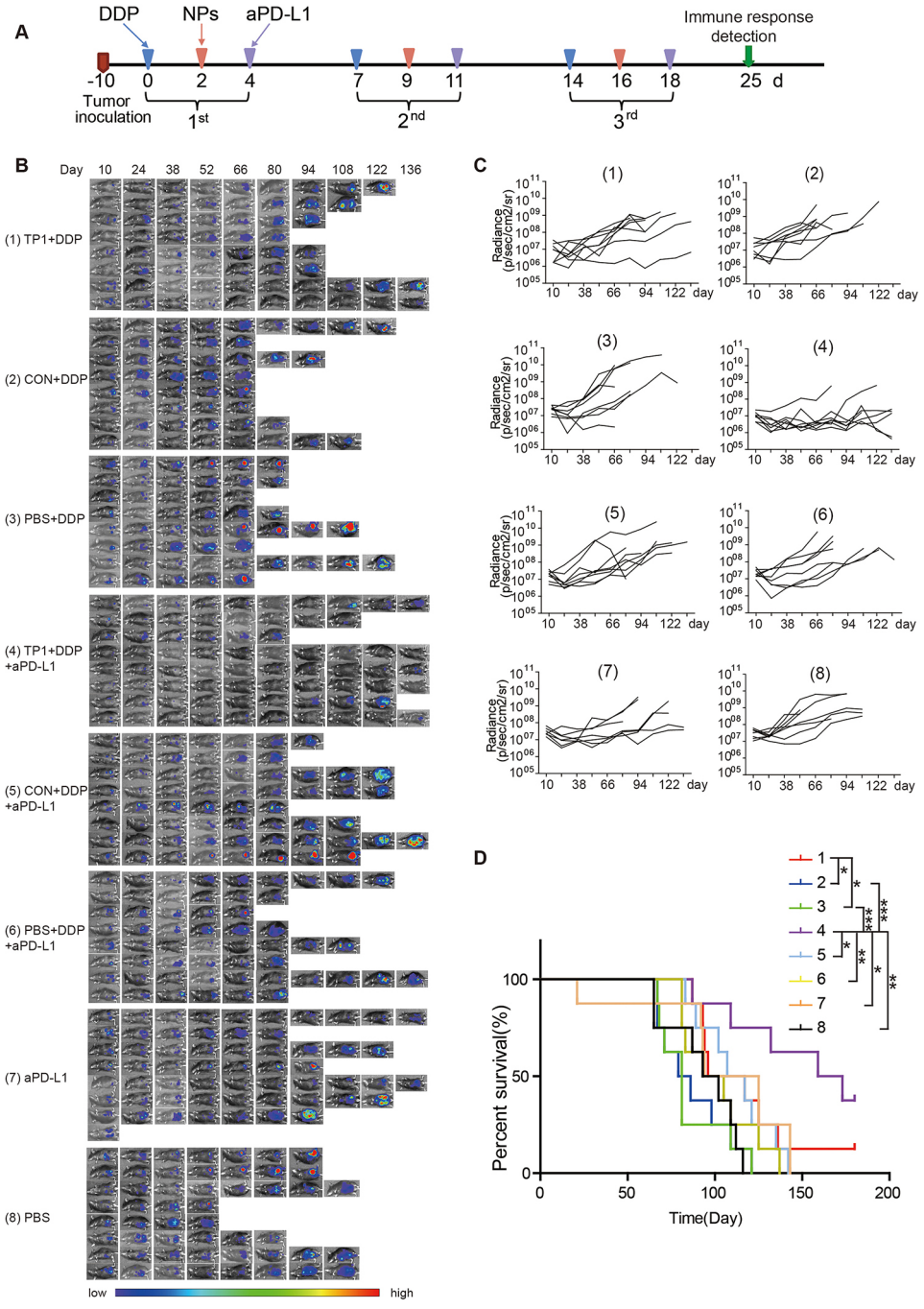

Fig. 6 Antitumor effect of nano-vaccines combined with DDP and aPD-L1. (**A**) Schematic illustration to show the experimental protocol of combination therapy. (**B**) Fluorescence images of ID8-luc tumor bearing mice treated with luciferase substrate over time after various treatment regimens. (**C**) The abdominal fluorescence signals of each mouse over time based on the imaging data shown in (**B**). (**D**) Survival of different groups of mice. P values were calculated by Log-rank (Mantel-Cox) Test (***$P < 0.001$, **$P < 0.01$ or *$P < 0.05$)

immunotherapy effect, and the combination of ICB aPD-L1 exhibited better immune activation.

To further prove that AC-NPs after antigen capture played the therapeutic role in vivo, we prepared AC-NPs in vitro and administered it to ID8 abdominal tumor-bearing mice to detect the therapeutic effect. Figure S6 showed the relevant result. The mice were treated with AC-NPs alone or in combination with aPD-L1, the administration mode was shown in Figure S6A. Figure S6B showed the survival of each group of mice. The survival of AC-TP1 alone or combined with aPD-L1 was significantly better than that of PBS group. However, there was no significant statistical difference in survival when compared with AC-CON or aPD-L1 group. On the one

hand, this was because both AC-CON and aPD-L1 had certain therapeutic effects; on the other hand, probably because the sample size was too small to make a statistical difference. In addition, lymphocytes were isolated from lymph nodes and spleen tissues for flow cytometry 7 days after the end of administration, and the proportions of CD4+T cells, CD8+T cells and Treg cells were detected respectively (Figure S6C). In both lymph node and spleen tissue, the proportion of CD8+T cells in AC-TP1-NP+aPD-L1 group was significantly higher than that in PBS group. In spleen tissue, the proportion of CD8+T cells in AC-TP1-NP+aPD-L1 group was also higher than AC-CON-NP group and aPD-L1 group, and the proportion of Treg in AC-TP1-NP+aPD-L1 group was significantly lower than that in PBS group. These results further confirmed the efficacy of AC-TP1-NP combined with aPD-L1 in the treatment of OCFurthermore, we examined the preventive effect of TP1-NP on OC after antigen capture. AC-TP1-NP and AC-CON-NP were prepared in vitro and administered to normal C57BL/6 mice for 3 cycles (Fig. 7A). The survival of mice was shown in Fig. 7B. The survival of mice prophylactically treated with AC-TP1-NP was significantly longer than those treated with AC-CON-NP or PBS. The proportion of activated DCs, CD4+T cells, CD8+T cells and Treg cells in lymph node tissue were shown in Figure S7. The proportion of CD4+T cells, CD8+T cells and Treg cells in spleen tissue were shown in Figure S8. These results indicated that AC-TP1-NP immunized mice had increased DC activation, increased effector T cells, and decreased inhibitory T cells. In particular, we examined the percentage of CD8+IFN-γ+cells and effector memory T cells (Tem, CD8+CD44+CD62L-) in spleen, which was thought to provide long-term immune protection [43, 49]. The IFN-γ producing CD8+cytotoxic T lymphocytes of AC-TP1-NP group were significantly more than AC-CON and PBS group (Fig. 7C). Similarly, the ratio of Tem in AC-TP1-NP group was significantly higher than in AC-CON and PBS group (Fig. 7D). These results demonstrated that AC-TP1-NP had not only a therapeutic but also a prophylactic effect on OC.

Biocompatibility is important for clinical transformation of TP1-NP. To examine the toxicity of nanoparticles in vivo, healthy C57BL/6 mice were administrated with the TP1-NP alone, combined with DDP, combined with DDP and aPD-L1 for three cycles, as shown in Fig. 6A. The mice were sacrificed at 14 days post-the last injection. Histological analysis of major organs showed that no signs of overt toxicity such as tissue degeneration or necrosis, compared to the effects of PBS on the treated mice (Figure S9). The results confirmed the nontoxicity and biocompatibility of TP1-NP and TP1-NP combination therapy.

Conclusion

Currently, the personalized vaccines are considered as a promising approach for assistant treatment after debulking surgery and chemotherapy in OC [50]. Numerous studies have shown the efficacy of therapeutic vaccines in OC. The recombinant pox-viral-based vaccine expressing tumor-associated antigen NY-ESO-1 showed clinical benefit among patients with OC [51]. P53-SLP vaccine combined with chemotherapy significantly promoted immune activation in vivo in several clinical studies [52, 53]. Immunogenic cell death of cancer cells can be induced by releasing DAMPs after chemotherapy in OC [30, 54]. By combining immunotherapy with chemotherapy, chemotherapy-induced apoptosis can be used as an adjuvant to synergistically enhance the anti-tumor immune response [55]. Although multiple studies have demonstrated an improved prognosis of vaccines for OC, these preclinical studies have not yet translated into clinical applications. This may be due to inappropriate antigen selection and the failure of tumor-specific T cells to homing in the tumor microenvironment [56]. The inter-individual and intraindividual molecular heterogeneity of OC determines that there is no readily available antigen for vaccine design. Herein, we described a platform for personalized cancer vaccines NP-TP1@M-M which hold the ability to capture tumor antigens. Due to the modification of tumor targeting peptide TMTP1, NP-TP1@M-M accumulated tumor antigens after chemotherapy in vivo and became a perfect vaccine antigen component. In addition, the modification of DC ligand mannose and the encapsulation of adjuvant MPLA further enhanced the immune activation efficiency of NP-TP1@M-M. Due to these characteristics and its nanoscale properties, NP-TP1@M-M after antigen capture showed enhanced immunostimulatory capacity, resulting in favorable therapeutic and preventive effect on OC when combined with chemotherapy and ICB. Personalized tumor vaccine designed with accurate and sufficient tumor antigens will be the research direction in the future. The treatment of OC has always been a challenge, but the antigen capture nano-vaccine NP-TP1@M-M in combination with chemotherapy offers a promising platform for improving survival of OC, especially when combined with ICB.

Materials and methods

Preparation and characterization of NP-TP1@M-M, NP-CON@M-M and corresponding AC-NPs

NP-TP1@M-M, NP-CON@M-M were prepared through the nanoprecipitation method. The precursor material PLGA-PEG-Mal and tumor targeting peptide TMTP1 modified material PLGA-PEG-TMTP1 were synthesized according to our previous synthesis route [24]. PLGA-PEG-Mal and mannosamine were dissolved in DMF at the molar ratio of 1:5, and reacting in water solution at

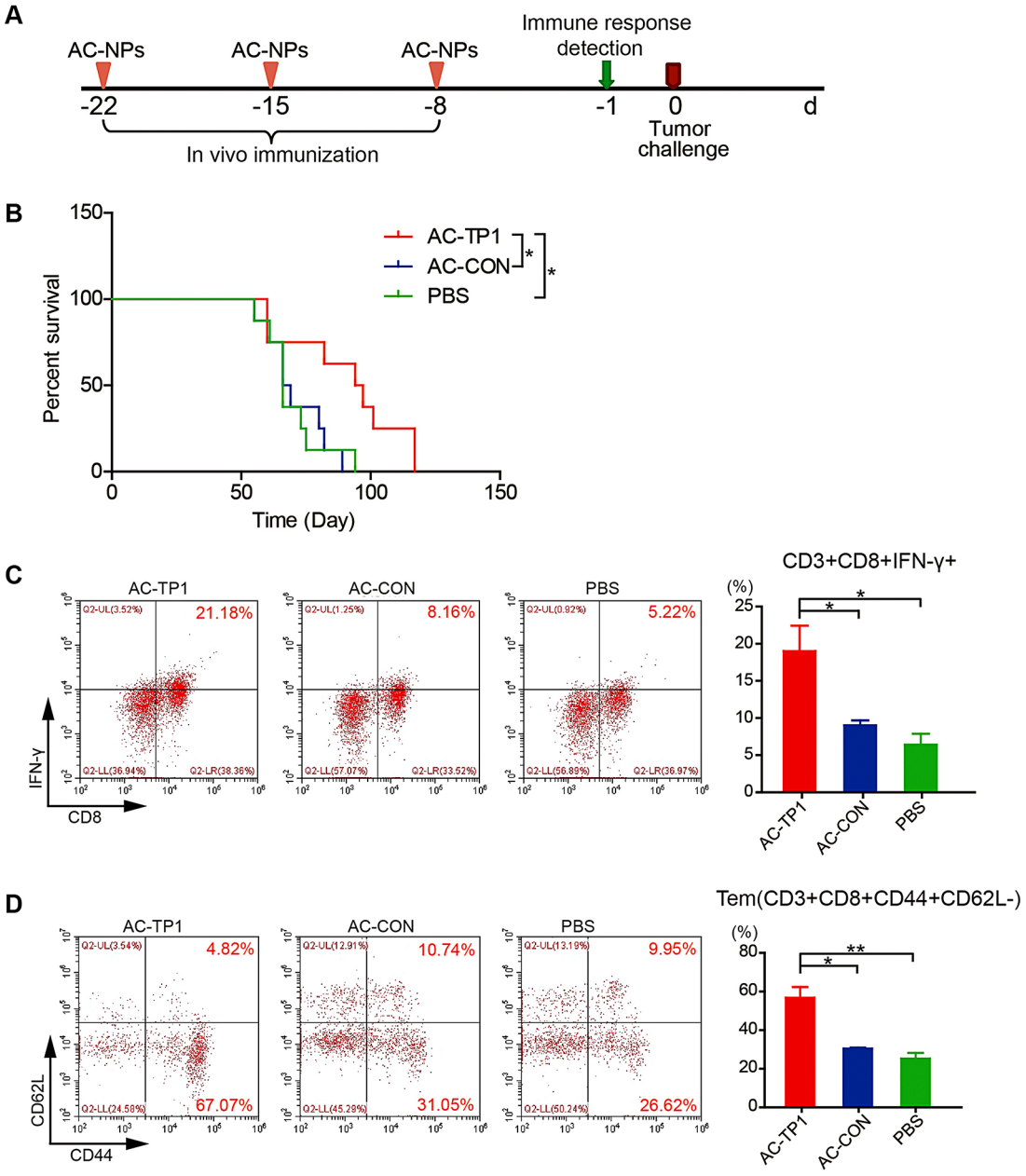

Fig. 7 Antitumor effect of AC-NPs as prophylactic vaccines. (**A**) Schematic illustration to show the tumor challenge experiment design. (**B**) Survival of different groups of mice. P values were calculated by Log-rank (Mantel-Cox) Test. (**C**) Representative flow cytometry plots of IFN-γ producing CD8 + cytotoxic T lymphocytes in spleen of different groups of mice and the corresponding proportion statistics. (**D**) Representative flow cytometry plots of effector memory T cells (Tem) in the spleen and the corresponding proportion statistics. (***$P < 0.001$, **$P < 0.01$ or *$P < 0.05$.)

40℃ for 24 h with magnetic stirring, followed by dialysis and lyophilization, then the mannose-modified material PLGA-PEG-Man was obtained. PLGA-PEG-TMTP1 and PLGA-PEG-Man were dissolved in 1 ml DMF at -a molar ratio of 1:2, 1:1 and 2:1 respectively with a total mass of 20 mg of the materials, and 200 μg MPLA was added. Then add the mixture drop by drop into 30 ml deionized water and stir magnetically for 30 min. Various proportions of NP-TP1@M-M were obtained by centrifugation at 12,000 rpm for 30 min. Then washed by distilled water and re-dispersed for future use. For control nanoparticle NP-CON@M-M, PLGA-PEG-TMTP1 was replaced by the control material mPEG2000-PLGA, and the preparation method was the same as above. Additionally, the coumarin-6 or DiR-labeled NP-TP1@M-M and NP-CON@M-M were prepared using a similar method by adding coumarin-6 200 μg or DiR 200 μg to the formulations.

To prepare AC-NPs, the tumor antigens from ID8 cells after chemotherapy was first prepared. ID8 cells

were treated with 80μmol/L DDP for 48 h and then the supernatant was collected and centrifuged at 1500 rpm for 5 min to remove dead cells and cellular debris. NP-TP1@M-M or NP-CON@M-M was incubated with the supernatant for 24 h. Specifically, 20 mg of each NPs was mixed with 10 ml of the tumor antigens from a T175 flask ID8 cells. Then the incubated solution was transferred to a 100kD ultrafiltration tube, and centrifuged at 12,000 rpm for 20 to 40 min. The AC-NPs were trapped above the ultrafiltration tube, and cell supernatant was below.

The hydrodynamic diameters of nano-vaccines were measured by dynamic light scattering (DLS, Brookhaven Instruments, USA). The morphology of nano-vaccines was characterized by transmission electron microscope (TEM, JEM-1230, Japan) without using any staining. The difference of protein content in tumor antigen solution before and after incubation was detected by the BCA assay, namely, the total amount of protein captured by nano-vaccines.

Identification of the species and abundance of tumor antigens captured by nano-vaccines in vitro

AC-NPs were prepared by the above method and sent to Wayen Biotechnologies (Shanghai) Inc. for protein spectrum detection. The extraction of tumor antigen proteins from AC-NPs was based on previous research [15]. The Precursor Intensity with Label-Free quantitative method was used for protein spectrum detection, the unique peptide segment was used to characterize the protein, and then the protein quantitative analysis was carried out according to the peak intensity of peptide segment related to primary mass spectrometry. When comparing AC-TP1-NP and AC-CON-NP, the ratio of peak intensity of the two was calculated. Differential proteins were defined as ratio≥4 or ≤0.25 and the number of unique peptides≥2. When the protein expression of the control group was 0, the ratio was assigned as 100. The tumor antigens was combined with previously published lists of tumor neoantigens, DAMPs and CAAs of OC [30, 31, 41].

Evaluation of dendritic cell activation and uptake

BMDCs were used to detect the activation effect of NPs and AC-NPs on DC. Bone marrow cells were harvested from the tibias of female C57BL/6 mice, and 20ng/ml GM-CSF and 10 ng/ml IL-4 were added into the medium to induce the differentiation of myeloid cells into DC cells. On day 8, cells were replated in 12-well and cultured for 24 h, then NPs and AC-NPs of various proportions were added respectively with a final concentration of 2 μg/ml. LPS was added as positive control, and the negative control without any stimulus. After 24 h incubation, cells were scraped, washed with cold PBS, and stained with anti-mouse antibody against CD11c-FITC, CD80-APC, CD86-PE (BioLegend) followed by flow cytometric analysis. The concentrations of cytokines IL-12p70, TNF-α and IFN-γ in DC medium supernatants were determined by ELISA following the manufacturer's protocol.

DC2.4 cells were used to detect the uptake of nanoparticles by DCs. Coumarin-6 labeled NPs and AC-NPs were incubated with DC2.4 cells for 30 min, washed with PBS for 3 times, and then observed under fluorescence microscope (Olympus IX73). The DC2.4 cells were also collected for flow analysis to further monitor the fluorescence intensity. In addition, nanoparticles with concentration gradients (12.5, 25, 50, 100, 200 μg/ml) were added into DC2.4 cells of 96-well plates, incubated for 48 h, and the cytotoxicity was detected by CCK-8 assay following the standard protocol.

Lymph nodes accumulation in vivo

Female C57BL/6 mice aged 5 weeks were randomly divided into 5 groups with 3 mice in each group, and 25ul, 10 mg/ml of NPs or AC-NPs coated with DiR were injected locally into the right foot pad, respectively. Free DiR of corresponding content was used as control group. NIR fluorescence images were collected under the IVIS Spectrum Imaging System (PerkinElmer) at 1 h, 2 h and 4 h after administration with an excitation wavelength of 745 nm and an emission wavelength of 800 nm. The mice were sacrificed after imaging, and the right popliteal, inguinal lymph nodes and major organs (heart, liver, spleen, lung and kidney) of the mice were isolated for ex vivo NIR imaging. The fluorescence radiation at the lymph nodes region was circled and measured by the ROI tool in the IVIS imaging software, and the curve of fluorescence intensity at the LNs of each group of mice was plotted over time.

Antitumor efficacy and in vivo immune response analysis

Firstly, luciferase expressed mouse ovary cancer cell ID8-luc was established by lentivirus vector, so that the tumor growth of abdominal cavity could be dynamically detected under IVIS system after the administration of luciferase substrate. ID8-luc cells were inoculated into the abdominal cavity of 5-week-old female C57BL/6 mice with 1×10^7 cells per mouse to construct the ID8 tumor bearing mouse model. On the 10th day after tumor grafting, 100 μl 2μmol/L DDP solution was intraperitoneally administered firstly. Two days later, 100 μl 10 mg/ml of the nano-vaccines were injected subcutaneously in the bilateral inguinal area, respectively. Then 100 μl 2.5 mg/ml of anti-mouse PD-L1 (clone:10 F.9G2, BioXcell) were intraperitoneally administered 2 days later. One week was one administration cycle, and a total of three cycles were administered. One week after the end of administration,

three mice in each group were sacrificed, and lymph nodes and spleen were separated for flow cytometry. Single cell suspensions were prepared and stained with a panel of the antibodies: FITC-antimouse CD3, APC-antimouse CD4, Cy5.5-antimouse CD8a, FITC-antimouse CD11c, APC-antimouse CD80, PE-antimouse CD86, PE-antimouse Foxp3, APC-antimouse IFN-γ (BioLegend). The remaining mice were imaged under the IVIS system every 2 weeks after giving luciferase substrate to evaluate the tumor growth. Death or abdominal circumference of the mice reaching 10 cm was defined as the end event. The ROI tool of imaging software was used to measure the fluorescence value of mice abdomen to indicate the abdominal tumor size.

To further test the therapeutic effect of AC-NPs, 100 μl 10 mg/ml AC-TP1-NP or AC-CON-NP was administered 10 days after implantation, and 100 μl 2.5 mg/ml aPD-L1 solution was administered intraperitoneally the other day. A 5-day dosing cycle lasted for 3 rounds. The immune response was measured one week after the end of administration. Detection of immune activation and monitoring of tumor growth and survival in mice were the same as above.

To detect the prophylactic effect of AC-NPs, normal female C57BL/6 mice were given three cycles of AC-NPs once a week at a dosage of 100 μl 10 mg/ml. 8 days after immunization, the mice were challenged with ID8 cells intraperitoneally and the survival were observed subsequently. 7 days after the last immunization, five mice from each group were dissect and the splenocytes and lymph nodes cells were collected for flow cytometry analysis. In addition to the above immune indicators, we also examined the levels of CD44 and CD62L to analyze the proportion of Tem.

Statistical analysis

Data were expressed as the means ± SEM. The results were analyzed by using an unpaired Student's t-test (two-tailed). The Kaplan-Meier method with the log-rank (Mantel-Cox) test were used for survival curve analysis. Values of $p<0.05$ were considered significant ($^{*}p<0.05$; $^{**}p<0.01$; $^{***}p<0.001$). P values were calculated by GraphPad Prism 5 and marked on the figures.

Associated content

Supporting information

The Supporting Information is available free of charge on the ACS Publications website: ^{1}H NMR spectrum of PLGA-PEG-Man, flow cytometry data for immune response detection in vivo, the determination of antitumor effect of AC-NPs, tables of qualitative and quantitative proteins captured by nano-vaccines detected by mass spectrometry.

Supplementary Information

The online version contains supplementary material available at https://doi.org/10.1186/s12951-024-02744-6.

Supplementary Material 1

Supplementary Material 2

Supplementary Material 3

Acknowledgements

This work was supported by the National Natural Science Foundation of China (82102884, 82172717, 82272628, 82002764).

Author contributions

Ling Xi, Xiangyi Ma, Ying Zhou designed the study. Ying Zhou and Rui Wei performed the experiments, conduct data analysis, and wrote original draft. Ling Wang, Jie Li, Wei Wang performed the animal experiments. Guiying Jiang, Xueqian Wang, Fei Li carried out the synthesis of nano-vaccines. Ling Xi, Xiangyi Ma and Songwei Tan guided and supervised proceed. Ling Xi and Xiangyi Ma reviewed and edited the manuscript. All authors read and approved the final manuscript.

Data availability

Data is provided within the manuscript or supplementary information files.

Declarations

Competing interests

The authors declare no competing interests.

Received: 11 December 2023 / Accepted: 2 August 2024
Published online: 13 August 2024

References

1. Reid BM, Permuth JB, Sellers TA. Epidemiology of ovarian cancer: a review. Cancer Biol Med. 2017;14(1):9–32.
2. Coukos G, Tanyi J, Kandalaft LE. Opportunities in immunotherapy of ovarian cancer. Ann Oncol. 2016;27(Suppl 1):i11–5.
3. Hamanishi J, et al. Safety and Antitumor activity of Anti-PD-1 antibody, Nivolumab, in patients with platinum-resistant ovarian Cancer. J Clin Oncol. 2015;33(34):4015–22.
4. Matulonis UA et al. Final results from the KEYNOTE-100 trial of pembrolizumab in patients with advanced recurrent ovarian cancer. J Clin Oncol, 2020. 38(15).
5. Varga A, et al. Pembrolizumab in patients with programmed death ligand 1-positive advanced ovarian cancer: analysis of KEYNOTE-028. Gynecol Oncol. 2019;152(2):243–50.
6. Disis ML, et al. Efficacy and safety of Avelumab for patients with recurrent or refractory ovarian Cancer phase 1b results from the JAVELIN Solid Tumor Trial. Jama Oncol. 2019;5(3):393–401.
7. Kershaw MH, et al. A phase I study on adoptive immunotherapy using gene-modified T cells for ovarian cancer. Clin Cancer Res. 2006;12(20):6106–15.
8. Chester C, et al. Immunotherapeutic approaches to ovarian cancer treatment. J Immunother Cancer. 2015;3:7.
9. Maeng H, Terabe M, Berzofsky JA. Cancer vaccines: translation from mice to human clinical trials. Curr Opin Immunol. 2018;51:111–22.
10. Paijens ST, et al. Antigen-specific active immunotherapy for ovarian cancer. Cochrane Database Syst Rev. 2018;9:CD007287.
11. Song W, Musetti SN, Huang L. Nanomaterials cancer Immunotherapy Biomaterials. 2017;148:16–30.
12. Allahyari M, Mohit E. Peptide/protein vaccine delivery system based on PLGA particles. Hum Vaccin Immunother. 2016;12(3):806–28.
13. Yang R, et al. Cancer Cell membrane-coated adjuvant nanoparticles with mannose modification for effective anticancer vaccination. ACS Nano. 2018;12(6):5121–9.

14. Koerner J, et al. PLGA-particle vaccine carrying TLR3/RIG-I ligand Riboxxim synergizes with immune checkpoint blockade for effective anti-cancer immunotherapy. Nat Commun. 2021;12(1):2935.
15. Min Y, et al. Antigen-capturing nanoparticles improve the abscopal effect and cancer immunotherapy. Nat Nanotechnol. 2017;12(9):877–82.
16. Lokhov PG, Balashova EE. Cellular cancer vaccines: an update on the development of vaccines generated from cell surface antigens. J Cancer. 2010;1:230–41.
17. Yang W, et al. TMTP1, a novel tumor-homing peptide specifically targeting metastasis. Clin Cancer Res. 2008;14(17):5494–502.
18. Liu R, et al. Enhanced targeted anticancer effects and inhibition of tumor metastasis by the TMTP1 compound peptide TMTP1-TAT-NBD. J Control Release. 2012;161(3):893–902.
19. Ma X, et al. DT390-triTMTP1, a novel fusion protein of diphtheria toxin with tandem repeat TMTP1 peptide, preferentially targets metastatic tumors. Mol Pharm. 2013;10(1):115–26.
20. Liu R, et al. The novel fusion protein sTRAIL-TMTP1 exhibits a targeted inhibition of primary tumors and metastases. J Mol Med (Berl). 2014;92(2):165–75.
21. Li F, et al. Evaluation of (99m)Tc-HYNIC-TMTP1 as a tumor-homing imaging agent targeting metastasis with SPECT. Nucl Med Biol. 2015;42(3):256–62.
22. McBride JW, et al. Development of TMTP-1 targeted designer biopolymers for gene delivery to prostate cancer. Int J Pharm. 2016;500(1–2):144–53.
23. Zhou Y, et al. A Novel Near-Infrared fluorescent probe TMTP1-PEG4-ICG for in vivo Tumor Imaging. Bioconjug Chem. 2018;29(12):4119–26.
24. Wei R, et al. TMTP1-modified Indocyanine Green-loaded polymeric micelles for targeted imaging of Cervical Cancer and Metastasis Sentinel Lymph Node in vivo. Theranostics. 2019;9(24):7325–44.
25. Jiang G, et al. TMTP1-Modified, Tumor Microenvironment Responsive nanoparticles Co-deliver Cisplatin and Paclitaxel Prodrugs for Effective Cervical Cancer Therapy. Int J Nanomed. 2021;16:4087–104.
26. Conibear AC, et al. Recent advances in peptide-based approaches for Cancer Treatment. Curr Med Chem. 2020;27(8):1174–205.
27. Zhong H, et al. Engineering peptide-functionalized Biomimetic Nanointerfaces for Synergetic capture of circulating Tumor cells in an EpCAM-Independent manner. Anal Chem. 2021;93(28):9778–87.
28. Ren J, et al. An engineered peptide tag-specific nanobody for immunoaffinity chromatography application enabling efficient product recovery at mild conditions. J Chromatogr A. 2022;1676:463274.
29. Wronska DB, et al. Peptide-conjugated glass slides for selective capture and purification of diagnostic cells: applications in urine cytology. Biotechniques. 2014;57(2):63–71.
30. Krysko DV, et al. Immunogenic cell death and DAMPs in cancer therapy. Nat Rev Cancer. 2012;12(12):860–75.
31. Paroli M, et al. Discovery of chemotherapy-associated ovarian cancer antigens by interrogating memory T cells. Int J Cancer. 2014;134(8):1823–34.
32. Bracci L, et al. Immune-based mechanisms of cytotoxic chemotherapy: implications for the design of novel and rationale-based combined treatments against cancer. Cell Death Differ. 2014;21(1):15–25.
33. Reed SG, Orr MT, Fox CB. Key roles of adjuvants in modern vaccines. Nat Med. 2013;19(12):1597–608.
34. Irache JM, et al. Mannose-targeted systems for the delivery of therapeutics. Expert Opin Drug Deliv. 2008;5(6):703–24.
35. Zhang YN, et al. Nanoparticle size influences Antigen Retention and Presentation in Lymph Node Follicles for Humoral Immunity. Nano Lett. 2019;19(10):7226–35.
36. Bachmann MF, Jennings GT. Vaccine delivery: a matter of size, geometry, kinetics and molecular patterns. Nat Rev Immunol. 2010;10(11):787–96.
37. Ali OA, et al. In situ regulation of DC subsets and T cells mediates tumor regression in mice. Sci Transl Med. 2009;1(8):8ra19.
38. Cairo CW, et al. Control of multivalent interactions by binding epitope density. J Am Chem Soc. 2002;124(8):1615–9.
39. Jule E, Nagasaki Y, Kataoka K. Lactose-installed poly(ethylene glycol)-poly(d,l-lactide) block copolymer micelles exhibit fast-rate binding and high affinity toward a protein bed simulating a cell surface. A surface plasmon resonance study. Bioconjug Chem. 2003;14(1):177–86.
40. Yin J, et al. Cyclic RGDyK conjugation facilitates intracellular drug delivery of polymeric micelles to integrin-overexpressing tumor cells and neovasculature. J Drug Target. 2011;19(1):25–36.
41. Castle JC, et al. Exploiting the mutanome for tumor vaccination. Cancer Res. 2012;72(5):1081–91.
42. Wang M, et al. NIR-Triggered Phototherapy and Immunotherapy via an Antigen-capturing nanoplatform for metastatic Cancer treatment. Adv Sci (Weinh). 2019;6(10):1802157.
43. Jin L, et al. In situ programming of Nanovaccines for Lymph Node-targeted delivery and Cancer immunotherapy. ACS Nano. 2022;16(9):15226–36.
44. Cruz LJ, et al. Targeting nanoparticles to dendritic cells for immunotherapy. Methods Enzymol. 2012;509:143–63.
45. Shi Y, et al. Dextran-polylactide micelles loaded with doxorubicin and DiR for image-guided chemo-photothermal tumor therapy. Int J Biol Macromol. 2021;187:296–308.
46. Armstrong DK, et al. Ovarian Cancer, Version 2.2020, NCCN Clinical Practice guidelines in Oncology. J Natl Compr Canc Netw. 2021;19(2):191–226.
47. Hamanishi J, et al. Programmed cell death 1 ligand 1 and tumor-infiltrating CD8 + T lymphocytes are prognostic factors of human ovarian cancer. Proc Natl Acad Sci U S A. 2007;104(9):3360–5.
48. Pawlowska A, et al. Immunotherapies based on PD-1/PD-L1 pathway inhibitors in ovarian cancer treatment. Clin Exp Immunol. 2019;195(3):334–44.
49. Chen Q, et al. A hybrid eukaryotic-prokaryotic nanoplatform with Photothermal modality for enhanced Antitumor Vaccination. Adv Mater. 2020;32(16):e1908185.
50. Tanyi JL et al. Personalized cancer vaccine effectively mobilizes antitumor T cell immunity in ovarian cancer. Sci Transl Med, 2018. 10(436).
51. Odunsi K, et al. Efficacy of vaccination with recombinant vaccinia and fowlpox vectors expressing NY-ESO-1 antigen in ovarian cancer and melanoma patients. Proc Natl Acad Sci U S A. 2012;109(15):5797–802.
52. Dijkgraaf EM, et al. A phase 1/2 study combining gemcitabine, Pegintron and p53 SLP vaccine in patients with platinum-resistant ovarian cancer. Oncotarget. 2015;6(31):32228–43.
53. Vermeij R, et al. Potentiation of a p53-SLP vaccine by cyclophosphamide in ovarian cancer: a single-arm phase II study. Int J Cancer. 2012;131(5):E670–80.
54. Bezu L, et al. Combinatorial strategies for the induction of immunogenic cell death. Front Immunol. 2015;6:187.
55. McCloskey CW et al. Ovarian Cancer immunotherapy: preclinical models and emerging therapeutics. Cancers (Basel), 2018. 10(8).
56. Tanyi JL, George E. Personalized vaccination against ovarian cancer: what are the possibilities? Expert Rev Vaccines. 2018;17(11):955–8.

Publisher's Note